

Synthesis and Characterization of Soluble Iron Oxide–Dendrimer Composites

Erica Strable,[†] Jeff W. M. Bulte,[‡] Bruce Moskowitz,[§] Kannan Vivekanandan,[†]
Mark Allen,[†] and Trevor Douglas^{*,†}

Department of Chemistry, Temple University, Philadelphia, Pennsylvania 19122-2585,
Laboratory of Diagnostic Radiology Research, National Institutes of Health,
Bethesda, Maryland, 20892-1074, and Institute for Rock Magnetism,
Department of Geology and Geophysics, University of Minnesota,
Minneapolis, Minnesota 55455

Received February 8, 2001

Carboxylated poly(amidoamine) PAMAM dendrimers (generation 4.5) have been utilized for the synthesis and stabilization of ferrimagnetic iron oxide nanoparticles. Oxidation of Fe(II) at slightly elevated pH and temperature results in the formation of highly soluble nanocomposites of iron oxides and dendrimer, which are stable under a wide range of temperatures and pH's. Size exclusion chromatography indicates aggregates in the 20–30-nm size regime, consistent with the oligomeric nature of the composite material. Transmission electron microscopy reveals small assemblies of mineral cores with electron diffraction and high-resolution TEM data, indicative of the mineral maghemite. SQUID magnetometry demonstrated that this crystalline composition exhibited superparamagnetism at room temperature. NMR relaxation studies of solvent (water) protons revealed unusually high T1 and T2 relaxivities, which make these materials excellent candidates as contrast agents for MR imaging.

Introduction

Recent work with poly(amidoamine) dendrimers has suggested that they can act effectively as organic matrixes for the synthesis of inorganic nanoparticles.^{1–11} Similar approaches utilizing functionalized organic arrays have been used previously to form nanoparticles by encapsulation within protein cages,^{12–14} polymer

matrixes,^{15,16} and surfactant vesicles.^{17–19} Previous work using the iron storage protein ferritin has shown that under appropriate synthetic conditions nanoparticles of magnetite or maghemite having a narrow size distribution can be synthesized within the confines of the protein cage.^{12,20,21} Ferritin is a spherical protein assembly surrounding a cavity 8 nm in diameter in which the iron oxide mineral is encapsulated.²² The inner surface of the assembly is characterized by the presence of clusters of carboxylic acids that act as mineral nucleation sites by virtue of their high charge density. The spatial selectivity afforded in the synthesis of ferritin-encapsulated nanoparticles is in part due to the unique chemical environment on the inner surface of the ferritin cage.^{12,13,23} In the present study we have used PAMAM dendrimers that represent a complemen-

* To whom correspondence should be addressed at: Department of Chemistry, Beury Hall, Temple University, Philadelphia, PA 19122-2585. Phone: (215)204-7916. Fax: (215)204-1532. E-mail: tdouglas@nimbus.temple.edu.

[†] Temple University.

[‡] National Institutes of Health.

[§] University of Minnesota.

(1) Zhao, M.; Sun, L.; Crooks, R. M. *J. Am. Chem. Soc.* **1998**, *120*, 4877–4878.

(2) Balogh, L.; Tomalia, D. A. *J. Am. Chem. Soc.* **1998**, *120*, 7355–7356.

(3) Zhao, M.; Sun, L.; Crooks, R. M. *Polym. Prepr. (Am. Chem. Soc., Div. Polym. Chem.)* **1999**, *40*, 400–401.

(4) Garcia, M. E.; Baker, L. A.; Crooks, R. M. *Anal. Chem.* **1999**, *71*, 256–258.

(5) Zhao, M.; Crooks, R. M. *Adv. Mater.* **1999**, *11*, 217–220.

(6) Sooklal, K.; Hanus, L. H.; Ploehn, H. J.; Murphy, C. J. *Adv. Mater.* **1998**, *10*, 1083–1087.

(7) Sooklal, K.; Huang, J.; Murphy, C. J.; Hanus, L.; Ploehn, H. J. *Mater. Res. Soc. Symp. Proc.* **1999**, *576*, 439–444.

(8) Huang, J. M.; Murphy, C. J. *Mater. Res. Soc. Symp. Proc.* **1999**, *560*, 33–38.

(9) Groehn, F.; Bauer, B. J.; Akpalu, Y. A.; Jackson, C. L.; Amis, E. J. *Macromolecules* **2000**, *33*, 6042–6050.

(10) Keki, S.; Torok, J.; Deak, G.; Daroczi, L.; Zsuga, M. *J. Colloid Interface Sci.* **2000**, *229*, 550–553.

(11) Esumi, K.; Hosoya, T.; Suzuki, A.; Torigoe, K. *J. Colloid Interface Sci.* **2000**, *226*, 346–352.

(12) Meldrum, F. C.; Heywood, B. R.; Mann, S. *Science* **1992**, *257*, 522–523.

(13) Meldrum, F. C.; Wade, V. J.; Nimmo, D. L.; Heywood, B. R.; Mann, S. *Nature* **1991**, *349*, 684–687.

(14) Douglas, T.; Young, M. *Nature* **1998**, *393*, 152–155.

(15) Ziolo, R. F.; Giannelis, E. P.; Weinstein, B. A.; O'Horo, M. P.; Ganguly, B. N.; Mehrotra, V.; Russell, M. W.; Huffman, D. R. *Science* **1992**, *257*, 219–23.

(16) Tang, B. Z.; Geng, Y.; Lam, J. W. Y.; Li, B.; Jing, X.; Wang, X.; Wang, F.; Pakhomov, A. B.; Zhang, X. X. *Chem. Mater.* **1999**, *11*, 1581–1589.

(17) Mann, S.; Hannington, J. P.; Williams, R. J. P. *Nature* **1986**, *324*, 565–567.

(18) De Cuyper, M.; Joniau, M. *Eur. Biophys. J.* **1988**, *15*, 311–19.

(19) Bulte, J. W. M.; de Cuyper, M.; Despres, D.; Frank, J. A. *J. Magn. Magn. Mater.* **1999**, *194*, 204–209.

(20) Douglas, T.; Bulte, J. W. M.; Pankhurst, Q. A.; Dickson, D. P. E.; Moskowitz, B. M.; Frankel, R. B.; Mann, S. *Inorganic-Protein Interactions in the Synthesis of a Ferrimagnetic Nanocomposite*; Mark, J. E., and Bianconi, P., Ed.; American Chemical Society: Washington, D.C., 1995; pp 19–28.

(21) Wong, K. K. W.; Douglas, T.; Gider, S.; Awschalom, D. D.; Mann, S. *Chem. Mater.* **1998**, *10*, 279–285.

(22) Harrison, P. M.; Arosio, P. *Biochim. Biophys. Acta* **1996**, *1275*, 161–203.

(23) Douglas, T.; Stark, V. T. *Inorg. Chem.* **2000**, *39*, 1828–1830.

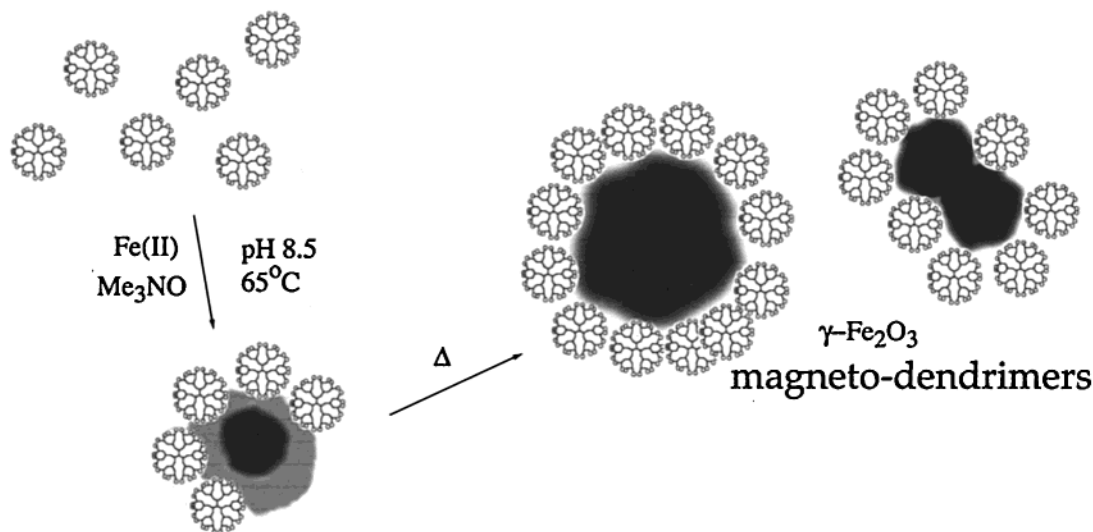


Figure 1. Schematic representation of the stabilization of maghemite nanoparticles by carboxyl-terminated poly(amidoamine) dendrimer (generation 4.5).

tary architecture to ferritin in that they are roughly spherical in shape but present a carboxylated surface on the *outside* of the spherical organic assembly. Our intention was to investigate the efficacy of these functionalized architectures in controlling the synthesis of iron oxide minerals under mild biomimetic conditions as outlined in Figure 1.

Here, we show that carboxylated poly(amidoamine) dendrimers can act to control the formation of well-defined ferrimagnetic iron oxide nanoparticles. In addition, the dendrimer acts to limit interparticle aggregation, possibly through surface passivation, and results in a highly soluble composite material. Oxidative hydrolysis at the dendrimer–solution interface, under controlled and mild synthetic conditions, leads to the formation of composite assemblies of dendrimer and inorganic mineral (Figure 1). These materials maintain their solubility over a wide range of conditions for extended periods of time. The magnetic behavior of these materials is consistent with superparamagnetic particles. The magneto-dendrimers were found to have unusually high T1 and T2 NMR relaxivities and are currently being explored as the basis for a new generation of contrast agents for magnetic resonance imaging applications.²⁴

Experimental Section

Magneto-dendrimer Synthesis. The carboxyl-terminated dendrimer (generation 4.5, Dendritech) (10 mg, 4×10^{-4} mmol) was added to the reaction vessel and the dendrimer solvent (methanol) was removed by a stream of N₂ for 20 min. Following this, 30 mL of deaerated H₂O (0.1 M NaCl, pH 8.5) was added and further deaerated by bubbling N₂ for 20 min and maintained under N₂ during the reaction. For an Fe loading of 100, deaerated solutions of (NH₄)₂Fe(SO₄) (25 mM, 1.58 mL, 4×10^{-2} mmol) and the two-electron oxidant Me₃NO (25 mM, 1.58 mL) were added at a fixed rate via a syringe pump. Fe(II) and Me₃NO solutions were added at rates of 1.58, 0.45, 0.21, or 0.105 mL/min. For syntheses of magneto-dendrimers with a loading factor of 50, 0.79 mL of Fe(II) (25 mM) and 0.79 mL of Me₃NO (25 mM) were used. For loading factors of 200, 3.16 mL of Fe(II) (25 mM) and 3.16 mL of

Me₃NO (25 mM) were used. The solution pH was maintained by titration of the H⁺ in a pH-Stat experiment using a Brinkmann 718 autotitrator. This eliminated the need to use contaminating buffers and allowed us to monitor the progress of the reaction. The change in pH was due in part to the acidic nature of the Fe(II) added and also due to H⁺ generated by the oxidative hydrolysis reaction to form the iron oxide mineral. After the completion of the reaction, Na₂Citrate was added (to 35 mM) to remove any unmineralized Fe. After reaction, the magneto-dendrimer product was dialyzed exhaustively against double-distilled H₂O and concentrated 50-fold by ultrafiltration (Amicon) using a 100 kDa *M_w* cutoff filter.

To determine the number of protons liberated during the reaction, controls were performed to determine the pH effects of reagent addition in the absence of reaction. Solutions of (NH₄)₂Fe(SO₄) (25 mM) were added to the 0.1 M NaCl/dendrimer reaction solution under anaerobic and oxidant-free conditions and the pH was maintained by autotitration. This control reaction was done in the presence of 2,2-dipyridine to prevent Fe(II) oxidation by adventitious O₂ and also allowed us to confirm that the Fe was indeed all in the 2+ oxidation state by virtue of the absorbance at 520 nm. Likewise solutions of Me₃NO (25 mM) were added to the 0.1 M NaCl/dendrimer reaction solution in the absence of Fe(II) and pH maintained by autotitration. The NaOH volume needed to adjust for any pH changes in controls were subtracted from the volume of NaOH needed to maintain pH stat conditions during the reaction. Standard (1.0 M) NaOH solutions were purchased (Aldrich) and diluted to working solutions of either 50 or 25 mM and standardized by titration against a primary standard of potassium hydrogen phthalate.

Attenuated total reflectance infrared spectroscopy (ATR-FTIR) of the reaction to form the magneto-dendrimers was accomplished using a liquid flow cell (Pike Technologies) with a ZnSe ATR crystal mounted into a Nicolet (Protégé 460) infrared spectrometer. During the reaction, liquid was pumped from the reaction vessel to the ATR flow cell at a rate of 200 μL/min and 64 scans were collected.

Characterization of Magneto-dendrimers. Size exclusion chromatography was performed using a column packed with Toyopearl 75-F resin (Supelco) and run on a BioLogic HR (BioRad) medium-pressure chromatography system. The flow rate in all experiments was 0.5 mL/min and the background buffer was 100 mM Tris, 150 mM NaCl, pH 7.5. Sample elution was monitored either at 405 nm or at 280 nm. The column was calibrated with large molecular weight standards of tobacco mosaic virus (*M_w* = 4×10^7), cowpea chlorotic mottle virus (*M_w* = 3.5×10^6), blue dextran (*M_w* = 2×10^6), and ferritin (*M_w* = 5×10^5).

(24) Bulte, J.; Douglas, T.; Strable, E.; Moskowicz, B.; Zywicke, H.; Frank, J., unpublished results.

The Fe content of magneto-dendrimer preparations was assessed using a Ferrozin-based spectrophotometric assay.²⁵ X-ray powder diffraction data were collected on a Rigaku dMax2 diffractometer and indexed using International Center for Diffraction Data (ICDD) diffraction files (39–1346 for maghemite). We could not unambiguously distinguish between maghemite (γ -Fe₂O₃, $a = 8.338$ Å) and magnetite (Fe₃O₄, $a = 8.377$ Å) because of the similarity in the lattice parameters. Samples were prepared for X-ray diffraction by extensive dialysis against double-distilled H₂O and subsequently dried under vacuum.

Magneto-dendrimer nanoparticles were imaged by transmission electron microscopy (TEM) using a Phillips 420 at 120 kV with a Kevex energy-dispersive X-ray analysis system. High-resolution TEM data were collected on a JEOL 4000FX microscope operating at 400 kV.

For SQUID magnetometry, 200- μ L solutions of magneto-dendrimer containing 62–662 μ g of Fe were placed in a superconducting quantum interference device (SQUID) susceptometer (Quantum Design). The magnetization was then measured over a field range -3 to $+3$ T (-30×10^3 to $+30 \times 10^3$ kOe) and at a temperature of 300 K. A sample holder correction was applied (subtraction of diamagnetic susceptibility) and moment calibration was performed using palladium and nickel standards. The measured magnetization was divided by the amount of iron, to yield specific magnetization (emu/g of Fe). Thermal demagnetization curves were obtained in the temperature range from 6 to 240 K after the magneto-dendrimer suspensions were initially frozen at 240 K. Samples were cooled in zero field to 5 K, given a saturation remanence in a field of 2.5 T, and then measured in an approximately zero field at 2 K intervals up to 240 K. The median blocking temperature of the system is taken as the temperature where 50% of the initial remanence has decayed.

Magneto-dendrimer samples for NMR relaxometry were adjusted to concentrations in the range 0.1–1.0 mM Fe. T1 and T2 were measured on a custom-designed variable-field relaxometer (Southwest Research Institute) at temperatures of 3 and 37 °C. For T1, 32 saturation-recovery sequences were used; T2 was measured with a CPMG sequence of 500 echoes with interecho time TE = 2 and 10 ms. The range of field strengths was 0.05–1.5 T. The data were converted to relaxation rates (reciprocals of T1 and T2); the background solution contribution was then subtracted and the result divided by the iron concentration to obtain relaxivity values (s⁻¹/mM Fe).

Results

We have synthesized stable suspensions of maghemite nanoparticles in the presence of carboxylated PAMAM dendrimers (generation 4.5). Using mild conditions of slightly elevated temperature (65 °C) and pH (8.5), oxidative hydrolysis of Fe(II) in the presence of the PAMAM dendrimers resulted in the formation of deep black-brown solutions that were stable in air for at least a year. The iron oxidation was achieved using (CH₃)₃NO as the oxidant. The reaction proceeded from a colorless solution through an intermediate green phase and finally to the brown solution, consistent with proposed pathways for the formation of the iron oxide phase magnetite or maghemite, proceeding through an intermediate “green-rust” phase.^{26,27} No bulk precipitate was observed in the reaction performed in the presence of the carboxylated dendrimer (generation 4.5) at Fe:dendrimer ratios up to 200. However, beyond that loading factor the dendrimer was no longer able to maintain the solubility of the maghemite nanoparticles

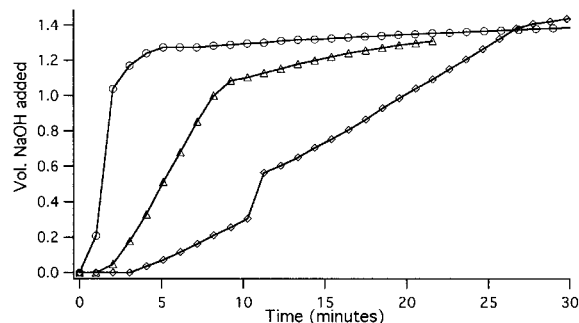


Figure 2. Titration of H⁺ generated by oxidative hydrolysis of Fe(II) in a pH-stat experiment. Reactants added over 1 min (○), 3.5 min (△), and 20 min (◇).

and bulk precipitation occurred. In control reactions, in the absence of the dendrimer, the reaction mixture rapidly formed a dark brown precipitate of maghemite. The reactions were all unbuffered and H⁺ generated by the oxidative hydrolysis of iron was titrated dynamically to maintain constant pH. Interestingly, attempts to perform the reaction using a buffer (100 mM HEPES, pH 8.5) rather than the pH-stat were unsuccessful and resulted in bulk precipitation. Control reactions in the absence of carboxyl-terminated dendrimer or in the presence of amine-terminated or hydroxyl-terminated dendrimers (generation 5) also resulted in the rapid formation of a dark brown precipitate with no stabilized soluble material. Repeated attempts to synthesize a stable colloidal composite using lower generation carboxyl-terminated dendrimers (generations 0.5, 1.5, 2.5, and 3.5) were unsuccessful over a wide range of Fe stoichiometries and reaction conditions. These reactions all resulted in the formation of a bulk precipitate of γ -Fe₂O₃ with characteristic X-ray powder diffraction.

The reaction to form the stable magneto-dendrimer with the generation 4.5 carboxyl-terminated dendrimers was investigated over a range of conditions including Fe:dendrimer stoichiometry (loading factor), rate of reagent (Fe and oxidant) addition, and the length of annealing time in solution after the addition of reagents.

Solutions of Fe(II) and oxidant were added over well-defined time periods, ranging from 1 to 30 min, into a reaction heated to 65 °C and maintained at pH 8.5 by means of an autotitrator which delivered small aliquots of NaOH to compensate for H⁺ released during the reaction and reagent addition. As shown in Figure 2, the oxidative hydrolysis reaction (followed by dynamic titration of H⁺ generated during the course of the reaction in a pH-stat experiment) occurred rapidly on the time scale of the reagent addition. A small, slow additional release of H⁺ could be noted after complete addition of Fe(II) and oxidant. In this way the reaction progress was monitored and ≈ 2 equiv of H⁺ were generated per Fe(II) as expected for the oxidative hydrolysis of a ferric oxyhydroxide. When followed spectrophotometrically (Figure 3), one can correlate the appearance of the green-colored intermediate with the rapid proton release from the initial oxidative hydrolysis. The appearance of the green color was followed by a slow transformation into the final mineral product having a characteristic broad visible absorbance consistent with the formation of the brown iron oxide.²⁷

The reaction was performed using Fe:dendrimer ratios of 50, 100, 200, and 250 with reagents being

(25) Stookey, L. *Anal. Chem.* **1970**, *42*, 779–781.

(26) Archibald, D. D.; Mann, S. *Nature* **1993**, *364*, 430–433.

(27) Schwertmann, U.; Cornell, R. M. *Iron oxides in the laboratory: preparation and characterization*, 2nd ed.; VCH: Weinheim, 2000.

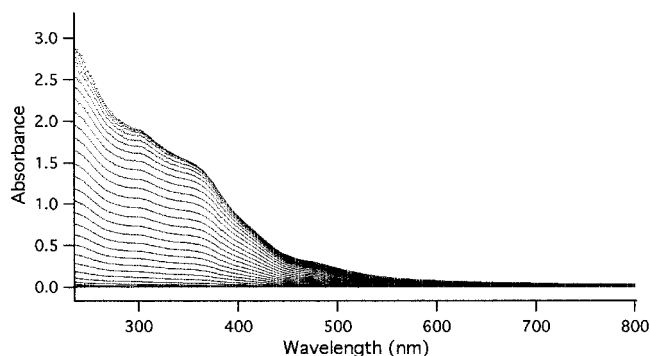


Figure 3. Change in absorbance during the synthesis of the magneto-dendrimer. The reaction proceeds from colorless to green after addition of Fe(II) and Me_3NO . As the reaction is heated, the color changes to an intense black-brown solution.

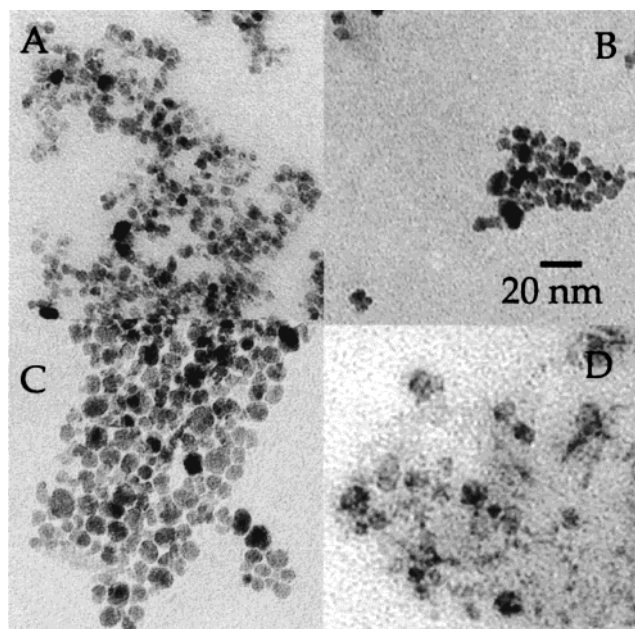


Figure 4. Transmission electron micrographs of magneto-dendrimer samples from synthesis with loading factors of (A) 50 Fe, (B) 50 Fe at twice the dendrimer concentration, (C) 100 Fe, and (D) 200 Fe (scale bar 20 nm).

added over the course of 20 min followed by an additional 40 min of heating at 65 °C. With Fe:dendrimer ratios up to 200 this reaction resulted in the formation of a homogeneous dark brown solution. These materials were quite stable to a wide range of conditions (pH 4–11 and temperatures up to 100 °C) for short periods of time without loss of solubility. However, at Fe:dendrimer ratios of 250 or above, the reaction resulted in precipitation of the iron oxide mineral well before the end of the 60-min reaction.

The mineral particles isolated from these reactions were imaged by transmission electron microscopy (TEM), which revealed fairly homogeneous particle sizes apparently aggregated into clusters (Figure 4). We suspect that these aggregates are largely the result of drying down effects in the TEM sample preparation. We observed no consistent correlation of aggregate size with sample preparation. However, because of the high contrast of the mineral particles, we could obtain some information regarding the individual mineral particles. At low loading factors (50 Fe per dendrimer) particles having an average diameter of 8.5 nm ($\sigma = 5$ nm) were

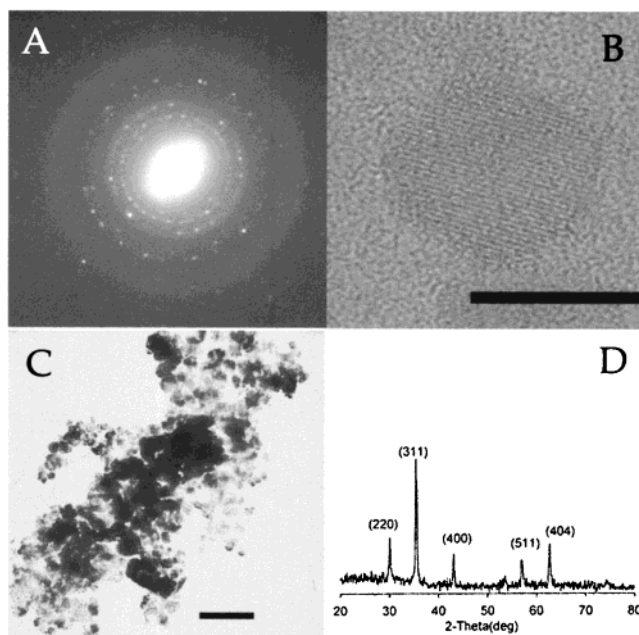


Figure 5. (A) Electron diffraction from an aggregate of particles. (B) High-resolution TEM of an individual particle showing $\{111\}$ lattice fringes ($d = 4.85$ Å) (scale bar 10 nm). (C) TEM of bulk precipitates formed in dendrimer free control reactions (scale bar 200 nm) and (D) X-ray diffraction of the control reaction precipitate.

observed (Figure 4A, B). Samples synthesized with a loading factor of 50 but under reaction conditions with 2-fold higher dendrimer concentrations produced virtually identical particles (Figure 4B). At a loading factor of 100 the particles were of highly consistent morphology with an average diameter of 9.5 nm ($\sigma = 5$ nm) as shown in Figure 4C. At higher loading factors (200 Fe per dendrimer) particles of similar average diameter (11 nm, $\sigma = 8$ nm) were observed but with a larger size distribution (Figure 4D). As shown by the electron micrograph, the magneto-dendrimer samples synthesized at a loading factor of 200 show far less well-defined particles and there is evidence for secondary nucleation in that many small particles are observed. Electron diffraction collected from the mineralized dendrimers (Figure 5A) revealed a powder pattern also consistent with a cubic iron oxide phase of magnetite or maghemite ($d = 2.96$ Å(220), 2.54 Å(311), 1.62 Å(511), 1.49 Å(440), and 1.09 Å(553)). High-resolution TEM (HRTEM) indicated the single-crystal nature of the mineral particles; $\{111\}$ (4.85 Å) lattice fringes could be identified and measured at 71° (Figure 5B). As shown in Figure 5C, precipitates formed in control reactions, which had been exhaustively dialyzed against ddH_2O , could be identified as the mineral phase maghemite on the basis of the X-ray powder diffraction (Figure 5D) by comparison with powder diffraction standards.

These mineralized dendrimer samples could be isolated and purified using size exclusion chromatography and characterized on the basis of their elution behavior, specifically their retention times. Prior to chromatography, the magneto-dendrimer samples were concentrated 50-fold by ultrafiltration (100 000 M_w cutoff). Concentration of the material in this way did not result in any loss of product through precipitation or passage through the ultrafiltration membrane. The concentrated and unconcentrated material were indistinguishable by

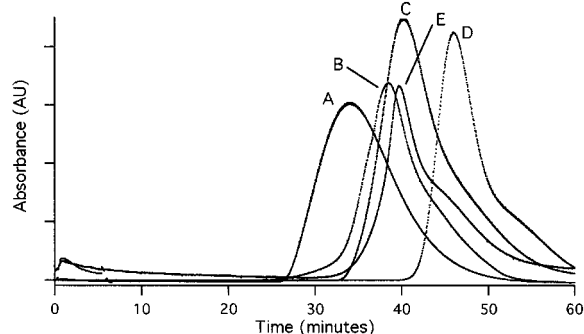


Figure 6. Size exclusion chromatography of magneto-dendrimer and molecular weight standards. Curve A is tobacco mosaic virus ($M_w = 40 \times 10^6$), B is cowpea chlorotic mottle virus ($M_w = 3.5 \times 10^6$), C is blue dextran ($M_w = 2 \times 10^6$), D is ferritin ($M_w = 5 \times 10^5$), and E is the magneto-dendrimer synthesized with 20-min reagent addition and 40-min annealing time.

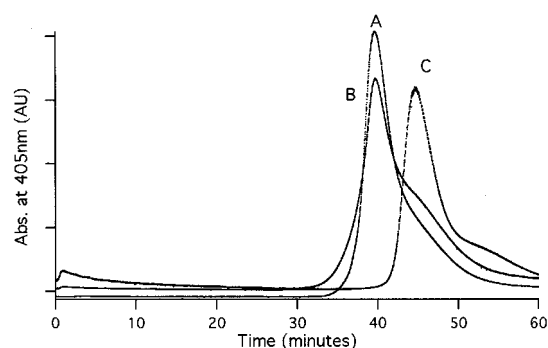


Figure 7. Size exclusion chromatography of magneto-dendrimers synthesized with 1-min reagent addition: (A) sample removed 60 min, (B) 10 min, and (C) 5 min after reagent addition.

size exclusion chromatography. As shown in Figures 6 and 7, solutions of the mineralized dendrimer eluted cleanly in a single peak on size exclusion chromatography and were monitored by the visible absorption of the iron oxide at 405 nm. When samples, made at different rates of reagent addition and at Fe loading factors, were chromatographed, virtually identical elution profiles were obtained. Using a size exclusion chromatography resin with a $5.0 \times 10^7 M_w$ exclusion limit (Toyopearl HW 75F) allowed us to analyze the magneto-dendrimer and roughly determine their solution particle size. Elution profiles of the magneto-dendrimer samples were compared to the elution of high molecular weight standards of tobacco mosaic virus ($M_w = 40 \times 10^6$), cowpea chlorotic mottle virus (26-nm diameter, $M_w = 3.5 \times 10^6$), blue dextran ($M_w = 2 \times 10^6$), and ferritin (12-nm diameter, $M_w = 4.5 \times 10^5$). As shown in Figure 6, the elution profile of the magneto-dendrimer lies between that of the cowpea chlorotic mottle virus and blue dextran. This suggests that the magneto-dendrimer structure lies in the 20–30-nm diameter range, possibly comprising more than a single mineral and dendrimer particle but almost certainly not the extensively aggregated material that the TEM images suggest.

Magneto-dendrimer synthesized with a loading factor of 100 (MD-100) gave the most consistent and reproducible particle formation and this stoichiometry has been used in subsequent studies as well as for all applications of this material involving magnetic resonance imaging.²⁴ Under conditions of constant Fe loading, the rate at

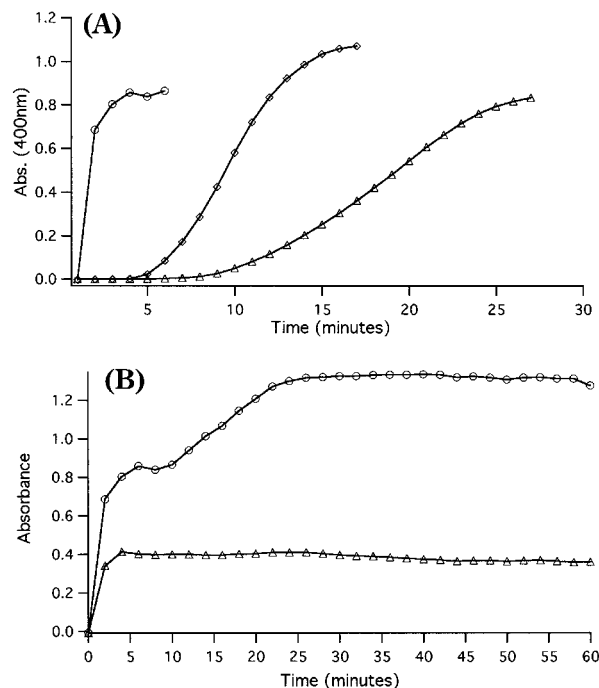
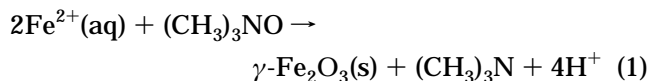


Figure 8. (A) Initial change in absorbance at 400 nm resulting from reactions where reagents were added over 1 min (○), 7.5 min (□), and 20 min (△). (B) Change in absorbance (at 400 nm (○) and 800 nm (△)) for magneto-dendrimer synthesized with 1-min reagent addition and 60-min subsequent annealing time.

which Fe(II) and oxidant were added to the reaction mixture was varied from 1 to 30 min. The physical properties of the resulting materials were investigated and are reported below. The resulting oxidative hydrolysis reactions were monitored through the release of protons that were titrated dynamically to maintain the reaction at pH 8.5. The titration profiles for reagent addition over 1, 7.5, and 20 min are shown in Figure 2. In all cases the rate of reagent addition is clearly rate determining. Upon addition of Fe(II) and oxidant there is an oxidative hydrolysis reaction which results in the liberation of protons according to reaction (1). The reactions gave consistent values of 2.2 ± 0.2 protons liberated per Fe. When these same reactions were



monitored by changes in the absorption spectrum in the UV–visible range, a similar reaction profile was observed (Figure 8). On the time scale of reagent addition there was a commensurate increase in the region of the spectrum associated with the formation of a μ -ferric oxo species (350–450 nm) characteristic of these iron oxide materials.^{27,28} As shown in Figure 8A, when the rate of reagent addition was varied between 1 and 20 min, there was an increase in the visible absorbance at 400 nm, which plateaued soon after all the reactant had been added. This correlates with a change in color from colorless, at the beginning of the reaction, to deep green observed after addition of all the Fe(II) and oxidant. At

(28) Cotton, F. A.; Wilkinson, G.; Murillo, C. A.; Bochmann, M. *Advanced Inorganic Chemistry*, 6th ed.; John Wiley & Sons: New York, 1999.

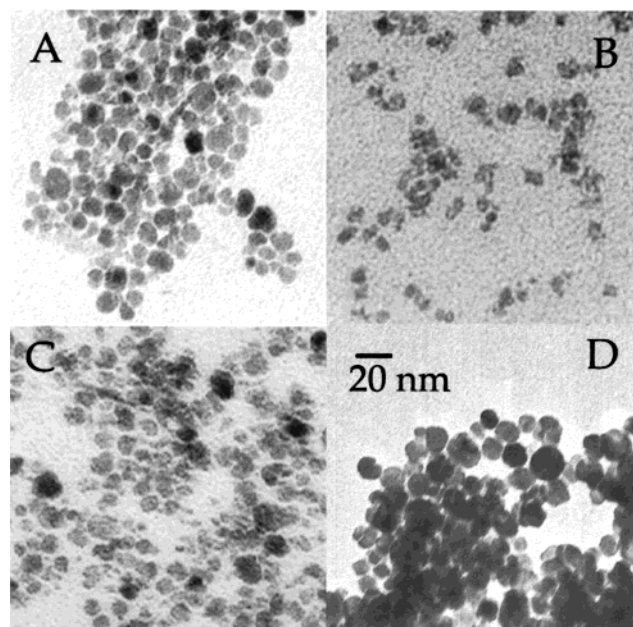


Figure 9. TEM of magneto-dendrimer samples synthesized by reagent addition over (A) 1, (B) 3.5, (C) 15, and (D) 20 min. Total reaction time in all cases was 60 min.

reaction times much beyond the reagent addition there was a further increase in the visible absorbance as the reaction slowly changed color from green to brown (see Figure 8B). When the reactions were allowed to proceed for a total time of more than an hour, there was a tendency of the reaction product to precipitate from solution. Interestingly, the reaction products from reactions where the rate of reagent addition was varied from 1 to 30 min (but the same total reaction time) showed very little difference when imaged by transmission electron microscopy. As shown in Figure 9 the average particle size for reactions with a 60 min total reaction time but rate of reagent addition varied between 1 and 20 min are all roughly 9–10 nm in average diameter. In addition, we could not resolve any significant differences in their elution behavior on size exclusion chromatography (Figure 7).

To investigate possible intermediate phases along the reaction path, we undertook the synthesis of the magneto-dendrimer (100 Fe loading) using the most rapid rate of addition at which our autotitrator could maintain pH-stat conditions (1-min reagent addition). We had previously shown that the end products of a 1-min reagent addition was morphologically not significantly different from the products synthesized under different rates of reagent addition. The reaction was monitored by the changes in the visible region of the spectrum. In addition, samples were removed at time intervals after the addition of Fe(II) and oxidant and the reaction quenched by the addition of citrate. Samples were removed 5 and 10 min after the addition of reagents and a final sample was collected when the reaction was stopped after 60 min.

As shown in Figure 8B, the visible absorption spectrum shows the development of a characteristic Fe–O absorbance (400 nm) on the time scale of reagent addition (1 min) and plateaus after 3–4 min. After 10 min there was a further increase in the absorbance at 400 nm, which plateaued after 20–25 min and remained

relatively flat until the end of the reaction. The second increase in visible absorbance was associated with the observed color change in the reaction from green to brown. It is of interest to note that the absorbance at the far end of the visible (800 nm) spectrum exhibited the same rapid increase in absorbance as that observed at 400 nm, reaching its maximum after roughly 5 min and remaining fairly constant throughout the reaction. This absorbance behavior is consistent with the formation of an initial phase which transforms into the final phase after roughly 30 min. The fact that the absorbance at both extremes of the visible spectrum do not increase with time is consistent with a nonaggregated material.

Size exclusion chromatography of the sample collected 5 min after reagent addition exhibited an elution profile very different from samples collected at later times after reagent addition. As shown in Figure 7, the elution profile of the 5-min sample had a longer retention time on the column and was therefore smaller in size than samples collected later in the reaction. Samples collected 10 min and later, all showed the same retention times. By comparison with available molecular weight standards, samples collected 10 min (and later) after addition of reagents all had retention times approximately between cowpea chlorotic mottle virus (26-nm diameter, $M_w = 3.5 \times 10^6$) and blue dextran ($M_w = 2 \times 10^6$). However, the sample collected 5 min after reagent addition had a retention time approximately the same as ferritin (12-nm diameter, $M_w = 5 \times 10^5$). With the size exclusion chromatography matrix used in these experiments we are able to clearly distinguish very large species, such as tobacco mosaic virus ($M_w = 40 \times 10^6$), from smaller species, such as blue dextran and ferritin. This technique does not give us the ability to distinguish small differences in particle size. However, even with the limited resolution of available size exclusion chromatography in this size range, we are able to clearly distinguish size differences between early intermediates in this oxidative hydrolysis reaction and those species observed toward the end of the reaction.

Transmission electron microscopy of samples isolated 60 min after the addition of reagents showed very well defined electron dense particles roughly 9.5 nm in diameter (Figure 10A). However, TEM images of the samples removed 5 and 10 min after reagent addition clearly show a marked difference from those collected at later times. As shown in Figure 10, these samples had significantly less electron dense material and were more diffuse than samples from later on in the reaction. The identifiable particles were measured and found to have average diameters of 4.6 nm ($\sigma = 3$ nm) and 5 nm ($\sigma = 3$ nm), respectively. This is consistent with the size exclusion chromatography characteristics described above in which the very earliest intermediate was significantly smaller in size than those at later times in the reaction.

The magnetic characteristics of samples taken from this reaction 10 and 60 min after addition of reagent were investigated by SQUID magnetometry and the data are shown in Figure 11. The magnetic behavior of these two materials were compared with a magneto-dendrimer sample synthesized using a 20-min addition of Fe(II) and oxidant and subsequently annealed for 40 min (MD-100). This latter material has been shown to

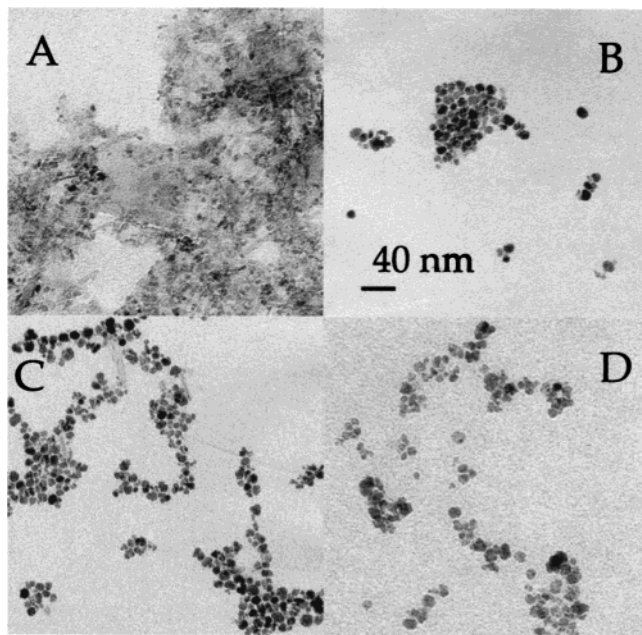


Figure 10. TEM of magneto-dendrimers synthesized by 1-min reagent addition and removed after (A) 5, (B) 30, and (C) 60 min. (D) MD-100 sample prepared by 20-min reagent addition and 40-min annealing time. Scale bar is 40 nm.

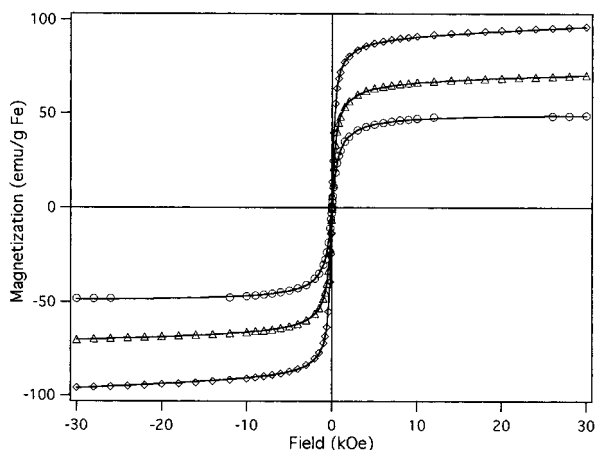


Figure 11. Magnetization of magneto-dendrimer samples and fit of the data to a Langevin function (solid line). MD-100 sample synthesized by 20-min reagent addition and 40-min annealing (\diamond); sample synthesized by 1-min reagent addition and 60-min annealing (Δ); sample synthesized by 1-min reagent addition and removed after 10 min (\circ).

Table 1. Calculated Magnetic Parameters

	M_{sat} (emu/g Fe)	T_{B} (K)	particle μ (BM)	particle d (nm)
10-min sample	50.8	17	14 400	8.8
60-min sample	68.6	21	23 200	10.3
MD-100	91.8	28	36 600	11.9

be a very effective contrast agent for magnetic resonance imaging.²⁴ The magnetization as a function of magnetic field strength is shown in Figure 11. The data were fit using a Langevin function assuming a uniform distribution of magnetic moments from 0 to μ_{max} . The calculated parameters are given in Table 1. The magnetic particle moment of the 60-min sample is nearly twice that of the 10-min sample, but not as high as MD-100 (Figure 11). The blocking temperature, above which the particle exhibits superparamagnetism (and that increases with

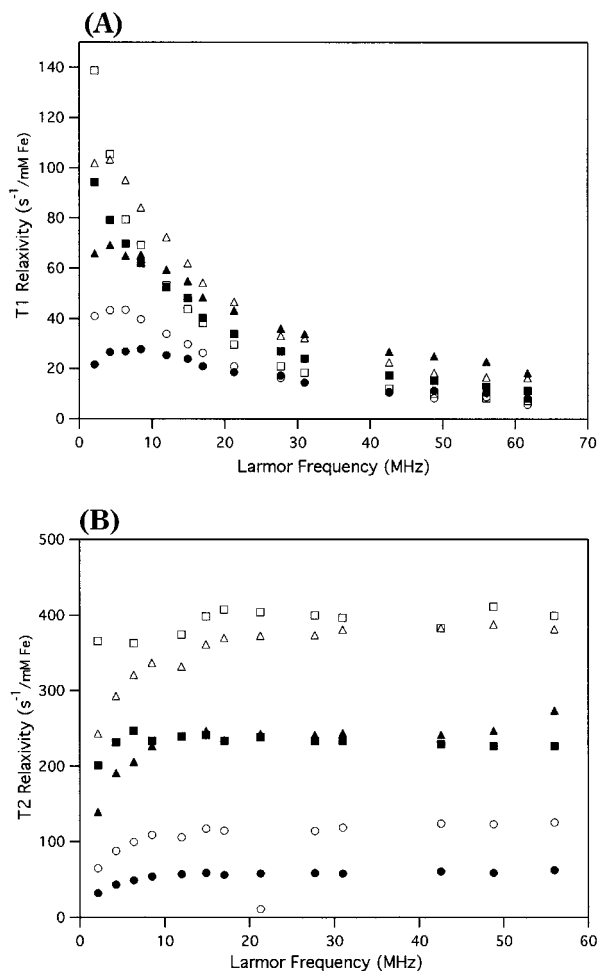


Figure 12. T1 (A) and T2 (B) relaxivities for magneto-dendrimer samples measured at 3 °C (open symbols) and 37 °C (solid symbols). MD-100 sample synthesized by 20-min reagent addition and 40-min annealing (\square , \blacksquare); sample synthesized by 1-min reagent addition and 60-min annealing (Δ , \blacktriangle); sample synthesized by 1-min reagent addition and removed after 10 min (\circ , \bullet).

particle size), is higher for MD-100 as compared to that of the 10-min sample, with the 60-min sample having an intermediate value (Table 1). The calculated particle diameters obtained from the Langevin function fits are in excellent agreement with those measured by TEM (with the 10-min sample being the smallest). All calculated parameters (including the saturation magnetization and particle magnetic moment) indicate that the magnetic properties of the 60-min sample are intermediate between the 10-min sample and MD-100. These data indicate that not all the iron in the 10- and 60-min sample particle has completely mineralized to pure maghemite. It also indicates that the sample prepared by slower addition, and subsequent annealing, results in nearly complete maghemite formation.

In addition, when the solution NMRD profiles of these samples were investigated, it was found that the T1 relaxivities dropped from 94 to 139 (MD-100), 66–102 (60-min sample), and 22–41 (10-min sample) at 2 MHz to 6–18 $\text{mM}^{-1} \text{s}^{-1}$ at 62 MHz (Figure 12A). At the lowest frequencies, there was no decrease in $1/T_1$ for MD-100, with a slight decrease but no full T1 relaxivity peak for the 60-min sample. The 10-min sample, however, exhibited a more pronounced peak of lower magnitude,

which is expected for smaller, less magnetic materials according to recently developed theories for (super)paramagnetic nanoparticles.^{29,30} The magnitude of the $1/T1$ at higher frequency is relatively low as compared to other magnetite-containing nanoparticles, likely as a result from a low surface-to-volume ratio (i.e., a larger particle oligomer).^{31,32} On the other hand, the measured $T2$ relaxivities (Figure 12B) demonstrate a saturation at a relatively low frequency (between 10 and 20 MHz), with unusually high values of 240–400 and 250–380 $\text{mM}^{-1} \text{s}^{-1}$ for the MD-100 and 60-min sample, respectively. Note that the 60-min sample is slower in reaching saturation as compared to the MD-100 sample, consistent with magnetometry results. The magnitude of the $1/T2$ data is typical of larger oligomeric structures in which the individual magnetic crystals act together as one, larger particle.^{31,32} On the other hand, the $T2$ relaxivities of the 10-min sample were significantly lower, between 63 and 125 $\text{mM}^{-1} \text{s}^{-1}$, in agreement with the smaller crystal size observed by TEM, chromatography, and magnetometry. There was no interecho time dependence for $1/T2$, indicating that the size regime of the mineralized dendrimers was well below the micrometer range.³³ Thus, the magnetic behavior of this material is consistent with a small oligocrystalline assembly in solution and can be manipulated by varying the reaction conditions.

It was found that there was a limit to the amount of time these materials could be heated under the reaction conditions before bulk precipitation was observed. In general, if the reaction was allowed to proceed for more than a total time of 60 min, bulk precipitation was observed. This could be due to cross-linking reactions between particles, leading to aggregation and bulk precipitation. Alternatively, thermal degradation of the dendrimer could result in an inability to stabilize the iron oxide colloid. To investigate the degradation of the dendrimer under the reaction conditions, we monitored the reactions in situ by attenuated total reflectance infrared (ATR-IR) spectroscopy, using a liquid cell and ZnSe crystal. Over the time course of the reaction (1 h), we noticed no decrease in the intensity of the amide peak at 3250 cm^{-1} or in control reactions where the dendrimer was subjected to the same conditions but in the absence of Fe(II). However, when the dendrimer solution was subjected to these conditions for 3 h, there was a measurable decrease in the intensity of the absorbance at 3250 cm^{-1} , implying dendrimer degradation. Therefore, in all the syntheses to make material suitable for application as contrast agents for MRI, reaction conditions were maintained to minimize long exposures to conditions that promote dendrimer degradation and subsequent precipitation; that is, no syn-

thesis was allowed to run past a total reaction time of 1 h.

A reversible particle aggregation of the magnetodendrimer solutions could be induced by the application of a high magnetic field gradient. This was achieved through application of a small CoSm magnet to the solution container, whereupon there was complete aggregation of all material. Upon removal of the magnetic field complete solubility was restored. This behavior is indicative of a soluble superparamagnetic material having no remnant magnetization at room temperature. In addition, these solutions could be freeze-dried to powders that redissolved completely upon addition of water.

Discussion

Our results suggest that the carboxyl-terminated generation 4.5 PAMAM dendrimers are very effective at stabilizing nanoparticles of iron oxide under the range of reaction conditions we have explored. The dendrimer could act to stabilize the particles in a number of ways. By virtue of the high charge density of its functionalized surface, the dendrimer is expected to assist nucleation through stabilization of embryonic aggregates. This would result in the formation of small particles. In addition, dendrimer-particle interactions might act to passivate the iron oxide surface and thus limit particle growth as well as block the interparticle interaction and aggregation as suggested in Figure 1. We observed only small differences in the average mineral particle size as a function of loading factor and no significant difference in the final mineral particle size as a function of the rate at which reagents are added to the reaction. These results suggest that in all cases our rate of addition is not sufficiently fast to significantly change the extent of initial particle nucleation. In the synthesis it appears that the particles are growth limited rather than nucleation limited. The fact that we see only small differences in average particle size even at different loading factors seems to suggest that the particles, once nucleated, grow to a fairly consistent size before their growth is spatially limited, presumably by the passivating dendrimer. In the samples made at the highest loading factor there is a significantly larger size distribution and clear evidence for many smaller particles. It is possible that the dendrimer provides some spatial limitation to the mineral particle growth and when that limit has been reached the system begins to re-nucleate. It appears that in our syntheses at loading factors up to 200 there is sufficient dendrimer present to passivate the mineral surfaces and maintain solubility. At loading factors above 200 there is simply not sufficient dendrimer present and the oxidative hydrolysis reaction leads to bulk precipitation through mineral cross-linking via an exposed mineral surface.

We were unable to synthesize a stable colloidal composite using lower generation carboxyl-terminated dendrimers (generations 0.5, 1.5, 2.5, and 3.5). These reactions all resulted in the formation of a bulk precipitate of $\gamma\text{-Fe}_2\text{O}_3$. This is a clear indication that the structure of the polymer, not merely the charged functional groups, are extremely important in the success of this reaction. This could be due to a more limited structural flexibility, and associated interaction

(29) Bulte, J. W. M.; Brooks, R. A.; Moskowitz, B. M.; Bryant, L. H., Jr.; Frank, J. A. *J. Magn. Mater.* **1999**, *194*, 217–223.

(30) Roch, A.; Muller, R. N.; Gillis, P. *J. Chem. Phys.* **1999**, *110*, 5403–5411.

(31) Bulte, J. W. M.; Vymazal, J.; Brooks, R. A.; Pierpaoli, C.; Frank, J. A. *J. Magn. Reson. Imaging* **1993**, *3*, 641–648.

(32) Bulte, J. W. M.; Brooks, R. A. *Magnetic Nanoparticles as Contrast Agents for MR Imaging*; Hafeli, U., et al., Eds.; Plenum Press: New York, 1997.

(33) Oligocrystalline materials of micron size have additional macroscopic field gradients which can dephase diffusing water molecules, over and beyond the usual spin-spin or dipole $T2$ relaxation mechanism, the effects of which increase with increasing interecho time.

with mineral surface, in the higher generation dendrimer as compared to the more open lower generation species. Lower generation dendrimers tend to exist in relatively open forms while the higher generation dendrimers adopt a more spherical structure. It is also possible that dendrimer–dendrimer interactions at the mineral surface play a role in determining the size of the final particle. In this regard, we are currently exploring the use of higher generation carboxyl-terminated dendrimers, now commercially available, as organic matrixes for the stabilization of metal oxide colloids.

On the basis of electrostatic considerations, the amine- and hydroxyl-terminated dendrimers would not be expected to have a significant effect on maghemite particle synthesis. The failure of PAMAM dendrimers with different functionalities ($-\text{NH}_2$, $-\text{OH}$) to stabilize the iron oxide particles is also consistent with a model where the dendrimer provides both a good nucleation surface as well as a strongly adsorbed passivating layer on the mineral surface. The bulk precipitation observed in dendrimer-free control reactions is presumably due in part to low nucleation density and extensive, unconstrained particle growth.

Reports suggest that the individual dendrimers are $\approx 4\text{--}5$ nm in diameter,^{34,35} roughly half the size of the iron oxide particles produced in this synthesis. Clearly, these iron oxide mineral particles are not entrapped within the dendrimer but rather grow from the dendrimer surface. Previous work using amino- or hydroxyl-terminated dendrimers to stabilize inorganic nanoparticles (Cu,^{1,2,36} Pt,^{3,5,36,37} Pd,^{3,36,37} Au,^{4,9,38} Ag^{10,11}) has relied in part on the affinity of the metal ions for the amine and possibly also the amide backbone. Thus, the dendrimer was preloaded with a precursor that was subsequently reduced to the zerovalent metal. This has resulted in metal nanoparticles localized both interior and exterior to the dendrimer. In reactions to form CuS³⁴ and CdS nanoparticles^{6,7,39} the appropriate dendrimers were initially charged with the metal ion and subsequently reacted with H_2S . The presence of the dendrimer stabilized the resulting colloid against bulk precipitation but not necessarily against particle aggregation.⁴⁰ In the present work, the highly charged

carboxylate interface presented by this structured polymer provides a surface very favorable for the stabilization of iron oxides. The maghemite nanoparticles appear to form from an initial green-rust-like material which in our experiments shows a different particle size very early on in the reaction. The particle size of this material changes rapidly, suggestive of an aggregation of dendrimer molecules around the embryonic particle which then matures into its final mineral form. This particle growth is borne out by the size exclusion chromatography, TEM, magnetometry, and NMR relaxivity data. However, it does not answer the question of whether the mineral nucleates at the highly charged dendrimer interface or in bulk solution followed by dendrimer aggregation to the growing mineral particle. The carboxylate functionality on the surface is clearly important for maghemite nanoparticle stabilization, but so too is the overall architecture of the dendrimer.

There is remarkably little difference in the size and morphology of the magneto-dendrimers synthesized at different rates of reagent addition. However, the magnetometry of samples prepared by 1-min addition and 60-min annealing are clearly different from those prepared by 20-min reagent addition and 40-min annealing. Even though the total reaction time is the same, the slower rate of addition seems to allow for a more fully crystalline maghemite particle. In a reaction performed under faster reagent addition, the lower saturation magnetization indicates the presence of non-maghemite iron oxide, which we were unable to detect by our diffraction techniques. It is possible that these preparations incorporate some amorphous material which results in lowered magnetization.

In summary, the multifunctional carboxyl-terminated PAMAM dendrimers (generation 4.5) provide a remarkable stabilizing effect on the synthesis of colloidal maghemite nanoparticles, which form soluble composite materials. This new class of materials have an unusually strong effect on T1 and T2 relaxation of solvent water protons, making them ideal candidates for further exploration as magnetic resonance imaging contrast agents, an area we are actively pursuing.

Acknowledgment. This research was partially supported by a grant from NSF (CHE-9801685) to T.D. The Institute for Rock Magnetism (IRM) is supported by grants from the Keck Foundation and the NSF.

CM010125I

(34) Tan, N. C. B.; Balogh, L.; Trevino, S. F.; Tomalia, D. A.; Lin, J. S. *Polymer* **1999**, *40*, 2537–2545.

(35) Nisato, G.; Ivkov, R.; Amis, E. J. *Macromolecules* **1999**, *32*, 5895–5900.

(36) Zhao, M.; Crooks, R. M. *Chem. Mater.* **1999**, *11*, 3379–3385.

(37) Zhao, M.; Crooks, R. M. *Angew. Chem., Int. Ed. Engl.* **1999**, *38*, 364–366.

(38) Esumi, K.; Hosoya, T.; Suzuki, A.; Torigoe, K. *Langmuir* **2000**, *16*, 2978–2980.

(39) Huang, J.; Sooklal, K.; Murphy, C. J.; Ploehn, H. J. *Chem. Mater.* **1999**, *11*, 3595–3601.

(40) Hanus, L. H.; Sooklal, K.; Murphy, C. J.; Ploehn, H. J. *Langmuir* **2000**, *16*, 2621–2626.